EVALUATING THE EFFICACY OF NEUTRAL DENSITY FILTERS AND CAMERA LENS APERTURE FOR REDUCING SENSOR SATURATION AND INCREASE IMAGE QUALITY IN DAYLIGHT EL IMAGING

Kabir Paúl Sulca[1]*, Rodrigo del Prado Santamaria[2], Thøger Kari[2], Julian Anaya[1], Gisele Alves dos Reis Benatto[2], Sergiu Viorel Spataru[2], Oscar Martínez[1]
[1]GdS-Optronlab group, Dpto. Física de la Materia Condensada, Universidad de Valladolid, Edificio LUCIA, Paseo de Belén 19, 47011 Valladolid (Spain)
[2]DTU Electro, Technical University of Denmark (DTU), Frederiksborgvej 399, 4000 Roskilde, Denmark.
*kabirpaul.sulca@uva.es

Daylight electroluminescence (dEL) inspection using InGaAs cameras has proven to be a powerful technique for assessing the condition of photovoltaic (PV) modules in the field. Recent advancements have shown it suitable for quality control and evaluation tasks in large-scale solar installations. The quality of dEL images is crucial for accurately identifying potential defects. Therefore, it is important to determine which camera optical stack yields stronger signals in dEL imaging. Camera optical stacks typically include specialized short-wave infrared (SWIR) lenses and bandpass filters to reduce background sunlight. To further limit the light intensity reaching the sensor and prevent saturation, options include adjusting the lens iris, using neutral density (ND) filters, or reducing exposure time. The choice among these depends on system constraints. Even though reducing exposure time is the easiest way to accomplish no saturation, high exposure time reduces noise, so ND filters and the iris are interesting options independent of the camera's internal controller. This study compares the light intensity reduction methods between ND filters and iris providing higher EL and dEL image quality using signal-to-noise ratio (SNR) as metric. Two SNR metrics (SNR_{kari} and $SNR_{(25)}$) are used to evaluate the configurations. We compare two setups: one using a C-RED 3 InGaAs camera with a SWIR lens (F-stop range 1.4–16) and a bandpass filter, and another using the same camera and lens fixed at F-stop 1.4 (fully open) combined with ND filters of varying transmittance (0.73 to 0.02). Indoor EL data is used to characterize light attenuation for each configuration. Subsequently, dEL images are captured under 600-800 W/m² irradiance for both setups. The results show that using the iris to reduce light intensity yields higher image quality. This is attributed to the increased depth of field resulting from a smaller optical aperture, which enhances the focus range and sharpness of the captured images. In conclusion, the study demonstrates that using a lens with an adjustable iris is more effective for dEL imaging with InGaAs cameras. This finding is valuable for optimizing optical setups to achieve high-SNR images in PV module inspections.

Keywords: Daylight Electroluminescence, InGaAs Camera, EL Signal-to-Noise Ratio, Photovoltaic Module Inspection.

1 INTRODUCTION

Photovoltaic (PV) module inspection is a critical task for ensuring the reliability and performance of PV solar energy systems [1,2]. Among the various diagnostic techniques available, daylight electroluminescence (dEL) imaging has emerged as a powerful method for detecting defects in PV modules under real-world operating conditions [3-8]. Unlike traditional electroluminescence (EL) imaging, which is typically performed indoors, dEL enables on-site inspection without the need for controlled lighting environments, making it highly suitable for large-scale solar installations.

The use of InGaAs cameras in dEL imaging has significantly enhanced the ability to capture high-quality images in the short-wave infrared (SWIR) spectrum [9-11]. However, achieving optimal image quality in daylight conditions remains a challenge, mainly due to the high noise caused by the ambient sunlight and the risk of sensor saturation, since sunlight intensity can be several orders of magnitude higher than EL intensity. Regarding the saturation problem, various optical components are employed to control the light intensity reaching the camera sensor, including neutral density (ND) filters, lens iris adjustments, and exposure time settings [10, 12].

Despite the reported use of these components, there is limited consensus on the most effective configuration for maximizing image quality while minimizing saturation. Reduced exposure time of the camera can solve directly this problem; however, using large exposure times can reduce certain types of CCD sensor noise [13]. In particular, read out noise is not increased with exposure time [13]. For these reasons, studying the efficacy of ND filters versus lens iris adjustments in reducing light intensity and enhancing image quality is of interest for EL and dEL in PV inspections. This issue has not been thoroughly investigated, thats why this study addresses this gap by evaluating the performance of these two approaches using signal-to-noise ratio (SNR) metrics ($SNR_{(25)}$ and SNR_{kari}) as indicators of image quality [11].

We evaluate the efficacy of ND filters and iris through a series of controlled indoor and outdoor experiments using a C-RED 3 InGaAs camera equipped with a SWIR lens and a bandpass filter. We use the previously described asynchronous method [9,11] with a fixed frequency and injection current to have comparable images. We analyze the impact of varying F-stop and ND filter transmittance levels on image quality and defect visibility. While, in general, all results obtained show sufficiently visible details there are clear differences between both setups.

The data presented consists in indoor and outdoor EL. We then analyze the experimental intensity reduction based on the indoor EL data. Even though iris steps are measured in F-stops, we can approximate each F-stop to a transmittance value to compare the two in terms of transmittance. Then, we present how the intensity attenuation works for indoor EL. Next, we calculate SNR values for EL and dEL providing an experimental insight on the quality of the images. Finally, ray tracing simulations provide deeper insight into the quality of each setup, rather than offering only a qualitative assessment of both setups.

10.4229/EUPVSEC2025/3AV.3.23
020191-001

2 EXPERIMENTAL DESCRIPTION

This study aims to evaluate the effectiveness of two optical configurations — lens iris adjustment and ND filters — in reducing sensor saturation and improving image quality in dEL imaging of PV modules. The methodology consists of indoor EL and outdoor dEL experiments conducted with a controlled optical setup, followed by dEL image processing and quality assessment using two metrics: $SNR_{(25)}$ and SNR_{kari} [11].

2.1 Optical Setup

The experimental procedure began with the characterization of ND filters. A spectral measurement in the 900–1500 nm range was performed to determine the transmittance percentage of each ND filter.

ND filter transmittance values were obtained from manufacturer data, while equivalent transmittance values for the iris were calculated based on the F-stop formula. Since each F-stop increment halves the aperture area, it was assumed that the light intensity reaching the sensor is also halved. Two optical configurations were tested:

a) Iris-based setup: The lens aperture varied using F-stop values of 1.4, 2.0, 2.8, 4, 8, and 16. The corresponding equivalent transmittance values, calculated from the F-stop relationship, were 1.00 t, 0.50 t, 0.25 t, 0.13 t, 0.03 t, and 0.01 t, respectively. These values served as reference transmittances.
b) ND filter-based setup: A fixed F-stop of 1.4 (fully open) was used in combination with ND filters with transmittance values of 0.73, 0.51, 0.20, and 0.15. Although spectral characterization revealed slight deviations from these values, those provided by the manufacturer datasheets were used for consistency. To explore a broader range of attenuation, combinations of two filters were also tested, resulting in additional transmittance values of 0.37, 0.152, and 0.02.

EL and dEL measurements were carried out using a C-RED 3 InGaAs camera with a resolution of 640 × 512 pixels, a pixel pitch of 15 × 15 µm, 14-bit quantization, a 16-bit dynamic range, and a maximum frame rate of 600 fps. The camera was equipped with a Kowa LM25HC-SW 25 mm SWIR lens and a bandpass filter centered at 1150 nm with a 50 nm full width at half maximum (FWHM).

2.2 Indoor EL and dEL measurements

Indoor EL images were captured to characterize the light attenuation properties of each optical configuration, obtaining a low-noise reference image which has been used to establish a reference SNR value. Although obtaining high-signal EL images was not necessary, the data were processed using the asynchronous image processing method to ensure consistent noise treatment across indoor EL and outdoor dEL measurements. This approach is essential for obtaining the $SNR_{(25)}$ metric, which is defined within the asynchronous processing framework.

The modulation parameters included a modulated current forming a square wave with a frequency of 6.25 Hz and an amplitude of 9.85 A, with the camera operating at 50 fps. Three exposure times (1, 2 and 3 ms) were tested to ensure sufficient signal, particularly under high-attenuation conditions.

Daylight EL images were acquired under medium irradiance conditions (600–800 W/m²) using the same modulated dEL technique. Exposure times of 1, 2 and 3 ms were also used to assess the impact of light reduction on image quality.

2.3 Image Processing

Image processing was performed using the asynchronous dEL processing algorithm defined in [11]. This method is designed to suppress noise and obtain a de-noised image. The number of sample images used to generate the final processed image was kept constant across all experiments to ensure comparability.

2.4 Image Quality Assessment

Image quality was quantified using two signal-to-noise ratio metrics: $SNR_{(25)}$ and SNR_{kari}.

a) as defined in [11], and $SNR_{(25)}$ value of above 10 is considered to be that of a high-quality image.
b) SNR_{kari}, described in [11], defines a good-quality image as one with an SNR value above 4.

Both metrics were applied to indoor and outdoor datasets to compare the performance of the iris-based and ND filter-based configurations.

2.5 Ray tracing simulations

Ray-tracing simulations were performed using the Optiland Python library. These simulations only model geometric optics and do not account for the wave nature of light or diffraction effects. The simulation uses the lens described in [14], with an initial F-stop of 2.0.

The ray-tracing model calculated the geometric light paths using ideal materials with refractive indices matching those of the actual lens. A 2D ray path was generated with y representing height and z the optical axis. Three-point light sources were simulated from an object plane located 2000 mm from the lens (z = −2000 mm). It was assumed the PV module to be parallel to the sensor, with (0, 0) corresponding to the center of both the panel and the sensor. The three source points were defined as follows:

- Point 1: (0, 0, −2000) mm.
- Point 2: (0, 550, −2000) mm.
- Point 3: (1100, 550, −2000) mm.

The x–y projection of the rays passing through the simulated lens onto the sensor plane was then plotted, and the number of rays reaching the sensor was quantified.

3 RESULTS AND DISCUSSION

3.1 Filter characterization

To ensure the quality and consistency of the intensity reduction provided by each ND filter, a spectral characterization was performed over the 900–1700 nm range. Ideally, the filters should exhibit approximately linear transmittance reduction behavior.

Figure 1 shows the measured counts across the spectral range and the corresponding relative transmittance (t), calculated relative to the “no filter” case.

We then compared the measured transmittance values with those provided by the manufacturer, as shown in Figure 2. Since the EL emission of the Si PV modules is centered around 1150 nm, particular attention was given to this wavelength. The measured transmittance values were found to be slightly lower than those reported in the manufacturer’s datasheet.

10.4229/EUPVSEC2025/3AV.3.23
020191-002

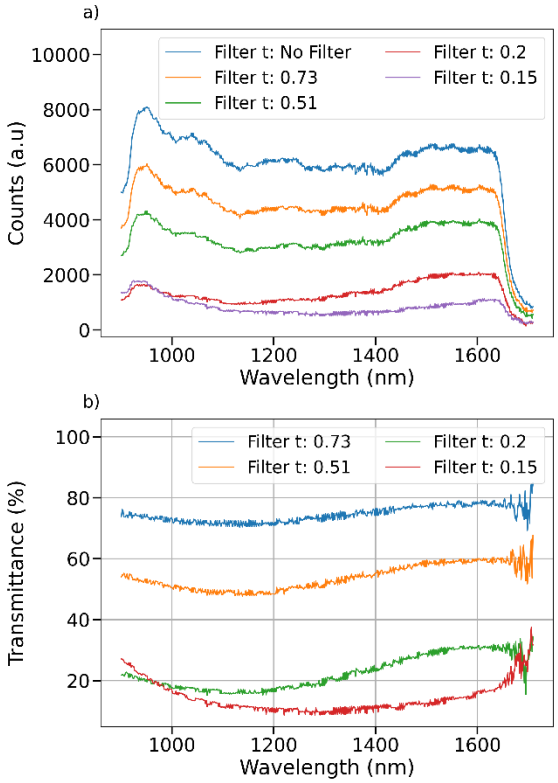

Figure 1: Filter transmittance in the 900-1700 nm range: a) counts (a.u), b) relative transmittance.

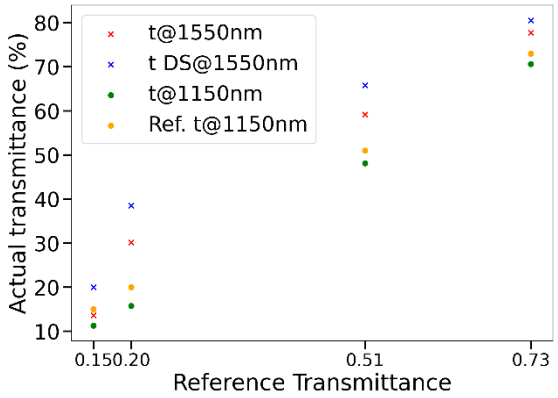

Figure 2: Reference transmittance vs measured transmittance percentage.

Since no significant differences were observed between the measured and reference transmittance values at 1150 nm, the reference values from the datasheet were used for subsequent analyses.

3.2 Indoor EL

An indoor dataset was acquired using both optical configurations: iris adjustment and ND filters. Figure 3 shows the EL images obtained under comparable conditions — 0.13 t (F-stop 4) for the iris and 0.15 t for the ND filter. The image captured with the iris shows uniform brightness and sharper detail, which improves visibility of small defects. The uniform brightness improvement can be attributed to reduced vignetting when the optical aperture is decreased. Vignetting is commonly caused by internal lens components. On the other hand, a sharper image can be attributed to an increase in depth of field and a reduction in optical artefacts due to the light´s geometrical paths within the lens´s internal arrangement . These F-stop effects are explored further in the simulation section.

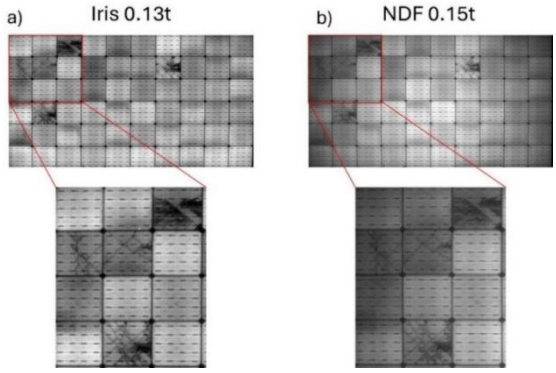

Figure3: Indoor EL image at 1 ms exposure time for a) 0.13 t iris aperture and b) 0.15 t ND filter

To analyze the behavior of light intensity reduction, the average pixel intensity was plotted as a function of transmittance (Figure 4). Both the iris and ND filters were found to effectively reduce the signal received by the sensor. Tests were conducted with exposure times of 1, 2 and 3 ms. A linear relationship was observed in the case of the ND filter (Figure 4b), whereas the iris case (Figure 4a) deviated from linearity, likely due to the simplifications made when estimating the equivalent transmittance.

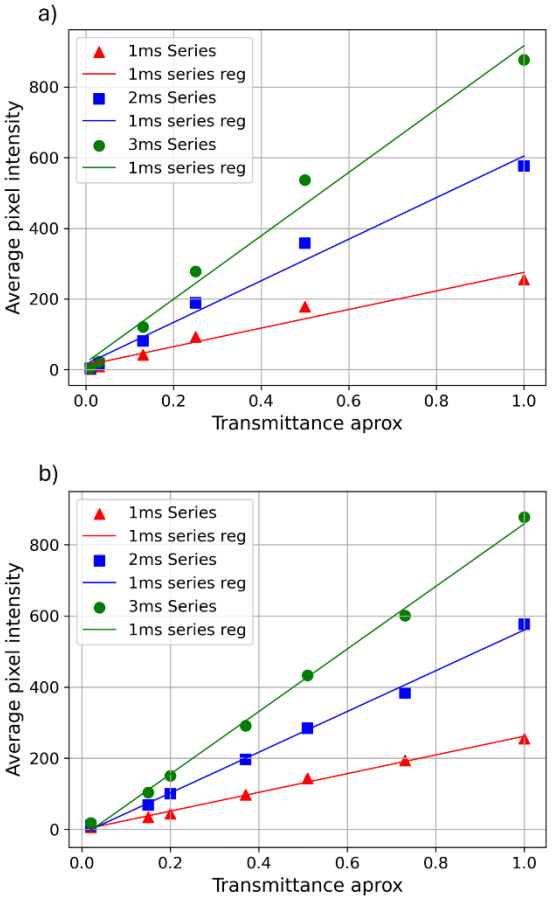

Figure 4: Average pixel intensity for a) iris aperture and b) ND filter, for 1, 2 and 3 ms exposure times

Next, we computed and plotted both SNR metrics for the indoor dataset (Figure 5). The iris configuration

10.4229/EUPVSEC2025/3AV.3.23
020191-003

consistently produced higher SNR values than the ND filter configuration. Interestingly, Figure 5b shows that the $SNR_{(25)}$ is higher at 0.5 transmittance (F-stop 2.0) than at 1.0 transmittance (F-stop 1.4). This suggests that the noise introduced by optical artefacts at larger apertures exceeds the contribution expected from a 50% reduction in signal. Regarding SNR_{kari}, this metric is less informative at high signal levels, as it was designed to address low-signal noise behavior.

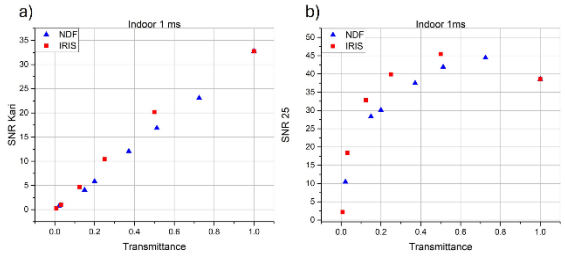

Figure 5: Indoor EL SNR for iris vs ND filter for 1 ms exposure time: a) SNR_{kari}, b) SNR_{25}.

3.2 dEL measurements

Daylight EL images were acquired and processed using the asynchronous method [11] under medium irradiance conditions (600–800 W/m²). Figure 6 shows the dEL images captured with a 1 ms exposure time for both configurations under similar conditions. While both images reveal most defects, the ND filter image exhibits vignetting, whereas the iris-based image shows sharper details and more uniform brightness, consistent with the indoor results.

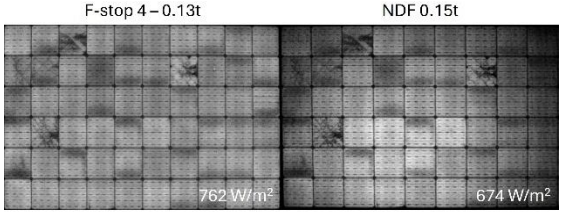

Figure 6: Daylight EL images obtained for similar intensity reductions using the iris (0.13 t) and the ND filter (0.15 t)

To quantitatively compare image quality, SNR metrics were computed for both setups (Figure 7). The iris configuration yielded higher SNR values, indicating stronger signals and better image quality. This can again be partially attributed to vignetting, as regions with lower intensity are interpreted as low-signal regions by the SNR metrics. Additionally, the same trend observed in the indoor experiments was reproduced: SNR values were higher at 0.5 transmittance (F-stop 2.0) and lower at 1.0 (F-stop 1.4). This supports the conclusion that, for the highest aperture, optical artefacts introduce more noise than signal is gained.

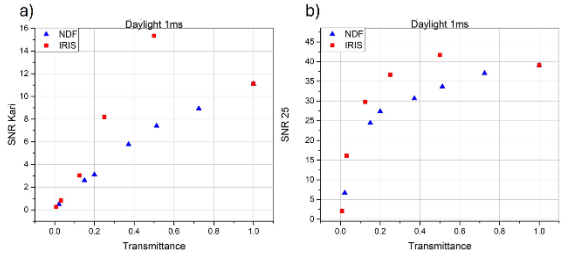

Figure 7: dEL SNR for iris vs ND filter for 1 ms exposure time: a) SNR_{kari}, b) SNR_{25}.

Overall, for both EL and dEL measurements, despite their methodological differences, both SNR metrics consistently indicate superior image quality when using the iris for all similar transmittance values. Higher SNR values indicate better data quality and more reliable signal detection from the images of the PV modules.

3.3 Ray tracing simulations

The simulation focused on three points of the PV module, as illustrated in Figure 8, with rays traced individually from each source point.

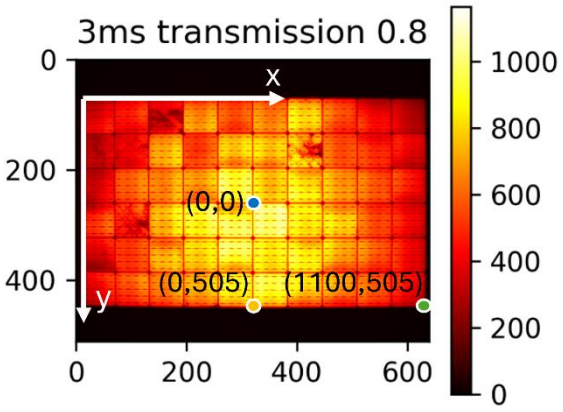

Figure 8: Ray tracing simulation source points scheme

We will study the rays reaching the final surface (sensor) only for the iris case because adding NDF to this kind of simulations will only linearly reduce the intensity without affecting the geometry of the setup. Figure 9 shows the (y,z) graph depicting the lens construction for a F-stop of 2.0 and the rays originating from the source points. We can observe the blue rays passing through the system from point (0,0), the orange rays from the point (0,550), and the green rays from the point (1100,550). We can also see the internal lens optic representation and sensor placement.

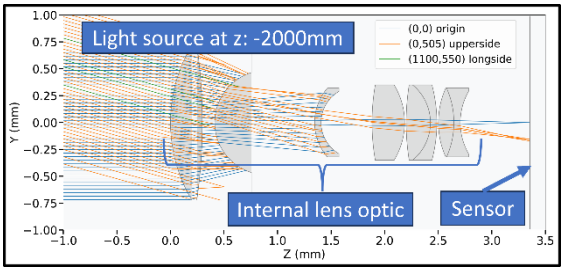

Figure 9: (y,z) internal optics and ray representations

An (x, y) projection of the sensor surface is shown in Figure 10, with normalized coordinates Hx and Hy. Normalization was performed relative to the longest sensor dimension.

We use the spot projection over the sensor to count the number of rays that reach the surface. We then make calculations for different F-stop values and plot the resultant rays that reach the sensor. Figure 11 shows the number of rays reaching the spot. The number of rays shows the expected tendency: a higher number of rays come from the origin, fewer from (0,550) and the fewest from the corner (1100,550). We can also observe that the difference between the sources is reduced when the aperture is closed; this is the same experimental pattern of

10.4229/EUPVSEC2025/3AV.3.23
020191-004

reduced vignetting.

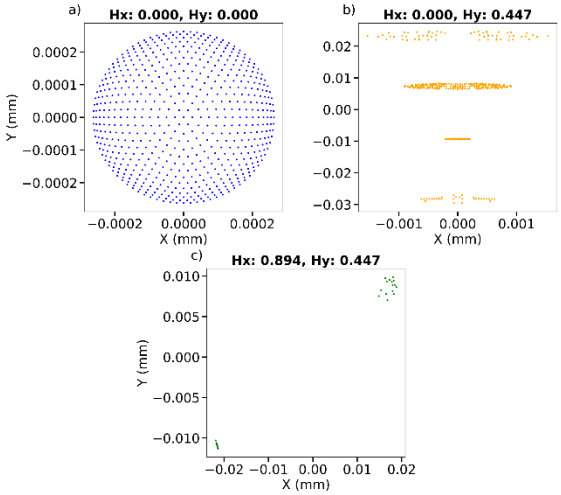

Figure 10: (x,y) ray tracing spot over sensor

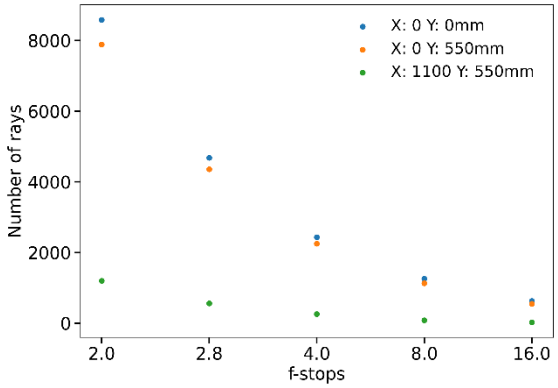

Figure 11: Number of rays for F-stops ranging from 2.0 to 16.0

To examine the vignetting effect further, a profile plot was generated along the x-direction from (0, 550) to (1100, 550) (Figure 12). The slope increases towards the sensor edges but decreases with smaller apertures.

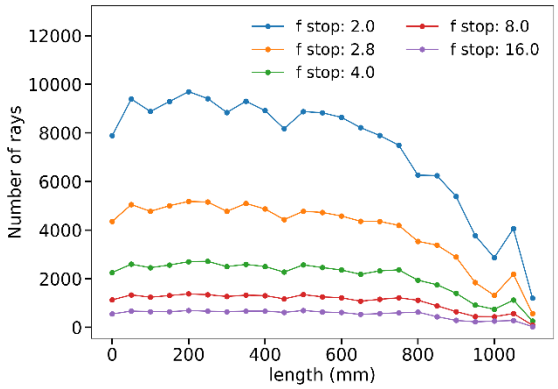

Figure 12: Profile plot for iris simulation

Lastly, we can observe the experimental profile plot in Figure 13. Half of the image is profiled, centered on the y-axis and along the x-axis. Notice how reducing the iris aperture flattens the reduction in intensity at the edges, whereas this does not happen as much with the neutral density filter.

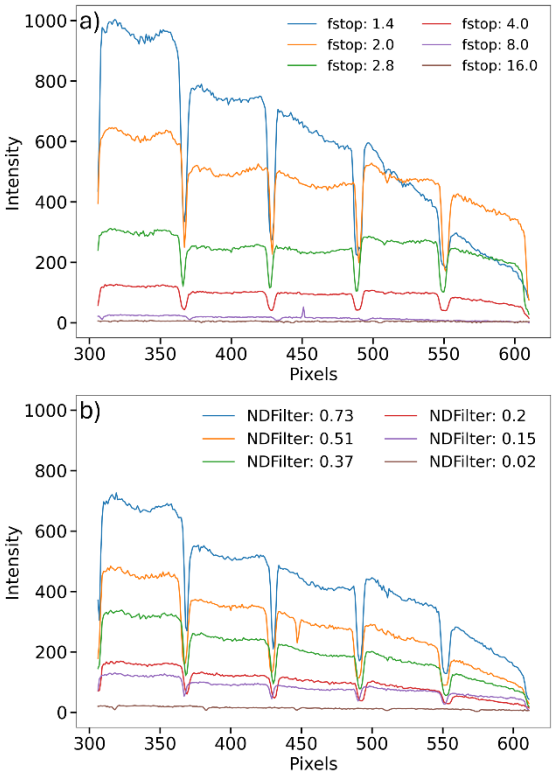

Figure 13: Experimental profile plot for F-stops (a) and ND filters (b)

4 CONCLUSIONS

This study systematically evaluated the effectiveness of neutral density (ND) filters versus lens iris adjustments in reducing sensor saturation and enhancing image quality in EL and dEL imaging of PV modules using InGaAs cameras. Through a combination of indoor EL characterization, outdoor dEL measurements, and ray tracing simulations, we demonstrated that adjusting the lens iris consistently yields superior image quality compared to using ND filters.

The comparative analysis revealed several important findings. First, adjusting the lens iris consistently produced higher SNR values across both SNR_{25} and SNR_{kari} metrics, indicating superior image quality and reduced noise. This improvement is attributed to the increased depth of field and reduced optical artefacts which can be related to the noise of the image and reduced vignetting associated with the signal. This results in enhanced image sharpness and uniformity. Second, ray tracing simulations supported these observations by showing that closing the iris leads to more evenly distributed light across the sensor, minimizing edge losses and optical artefacts. Third, the characterization of ND filters revealed discrepancies between manufacturer-stated and actual transmittance values, particularly at lower transmittance levels, which may introduce inconsistencies in image quality. Taken together, these findings demonstrate that iris-based light attenuation not only improves image clarity but also ensures more reliable and consistent imaging performance in both EL and dEL applications.

10.4229/EUPVSEC2025/3AV.3.23
020191-005

5 ACKNOWLEDGMENTS

This work has been funded by the Spanish Ministry of Science and Innovation, under project PID2023-148369OB-C43, financed by MICIU/AEI /10.13039/501100011033 and FEDER/UE, and by the Regional Government of Castilla y León (Junta de Castilla y León) and by the Ministry of Science and Innovation and the European Union NextGenerationEU / PRTR under the project "Programa Complementario de Materiales Avanzados". K. Sulca has been funded under the call for predoctoral contracts UVa 2022, co-financed by Banco Santander.

6 REFERENCES

[1] L. Koester, S. Lindig, A. Louwen, A. Astigarraga, G. Manzolini, D. Moser, Renew. Sustain. Energy Rev. 165 (2022) 112616.
[2] I. Høiaas, K. Grujic, A. Gerd, I. Burud, E. Olsen, N. Belbachir, Renew. Sustain. Energy Rev. 161 (2022) 112353.
[3] L. Stoicescu, M. Reuter, J.H. Werner, Proceedings 29th Eur. Photovolt. Sol. Energy Conf. Exhib., (2014) 2553.
[4] J. Adams, B. Doll, C. Buerhop, T. Pickel, J. Teubner, C. Camus, C.J. Brabec, Proceedings 32nd Eur. Photovolt. Sol. Energy Conf. Exhib., (2015) 1837.
[5] S. Koch, T. Weber, C. Sobottka, A. Fladung, P. Clemens, J. Berghold, Proceedings 32nd Eur. Photovolt. Sol. Energy Conf. Exhib., (2016) 1736.
[6] G.A. dos Reis Benatto, N. Riedel, S. Thorsteinsson, P.B. Poulsen, A. Thorseth, C. Dam-Hansen, C. Mantel, S. Forchhammer, K.H.B. Frederiksen, J. Vedde, M. Petersen, H. Voss, M. Messerschmidt, H. Parikh, S. Spataru, D. Sera, Proceedings 44th IEEE Photovolt. Specialist Conf., (2017) 2682.
[7] M. Guada, A. Moretón, S. Rodríguez-Conde, L.A. Sánchez, M. Martínez, M.A. González, J. Jiménez, L. Pérez, V. Parra, O. Martínez, Energy Science & Engineering 8 (2020) 3839.
[8] O. Kunz, J. Schlipf, A. Fladung, Y.S. Khoo, K. Bedrich, T. Trupke, Z. Hameiri, Prog. Energy 4 (2022) 042014.
[9] C. Terrados, D. G. Francés, J. Anaya, K.P. Sulca, V. Gómez-Alonso, M. A. González, O. Martínez, Daylight Photoluminescence of Silicon Solar Panels In Operation by Electrical Modulation, Proceedings of the 40th EUPVSEC, Vol I (2023) 258.
[10] Dhimish, M., & Tyrrell, A. M., Optical Filter Design for Daylight Outdoor Electroluminescence Imaging of PV Modules. In Photonics, Vol. 11, No. 1, p. 63 (2024). MDPI.
[11] G. A. dos Reis Benatto, T. Kari, R. del Prado Santamaría, S. V. Spataru, C. Terrados, D. G. Francés, J. Anaya, K. P. Sulca, V. Gómez-Alonso, M. A. González, O. Martínez, Daylight Electroluminescence Imaging Methodology Comparison, Proceedings of the the 40th EUPVSEC Vol I (2023) 374.
[12] G. A. dos Reis Benatto, T. Kari, R. del Prado Santamaría, A. Mahmood, L. Stoicescu, S. V. Spataru, Evaluation Of Daylight Filters For Electroluminescence Imaging Inspections Of C-Si Pv Modules, Proceedings of the 41st EUPVSEC, Vol I (2024) 2163
[13] Fellers, T. J., and M. W. Davidson. Concepts in Digital Imaging Technology, CCD Noise Sources and Signal-to-Noise Ratio. (2010).
[14] Laikin, M. Lens Design. Optical science and engineering series, 4th ed, (2007) 101.